SHORT COMMUNICATION

Contact electrification at the solid–liquid transition interface

Yu Wei [a,b,1], Xiang Li [a,b,1], Zhe Yang [a,b], Jiajia Shao [a,b], Zhong Lin Wang [a,c,d,*], Di Wei [a,*]

[a] Beijing Institute of Nanoenergy and Nanosystems, Chinese Academy of Sciences, Beijing 101400, China
[b] School of Nanoscience and Engineering, University of Chinese Academy of Sciences, Beijing 100049, China
[c] Guangzhou Institute of Blue Energy, Knowledge City, Huangpu District, Guangzhou 510555, China
[d] Georgia Institute of Technology, Atlanta, GA 30332-0245, United States

Contact electrification (CE) is a well-known phenomenon that ubiquitously exists in the charge transfer between solid–solid (S-S) or solid–liquid (S-L) and plays pivotal roles in energy harvesting and self-powered sensing. However, little is known about the CE mechanism during the phase transition. Here, we investigated the mechanism of charge transfer between a representative crystalline ice and a dielectric material during the solid-to-liquid phase transition. This study aimed to determine how the phase transition affects the charge transfer efficiency. Before ice starts melting, electron transfer within S-S contact predominated. As the melted micro-droplets smoothed the rough surface of the ice, the contact area between the materials increased, resulting in a roughly 6-fold enhancement of charge transfer. When the ice melted, droplets condensed on the surface and established S-L contact with the dielectric material. It resulted in the formation of an electrical double layer (EDL) composed of ions and electrons at the contact interface, effectively shielding the surface net charge of the dielectric material and impeding charge transfer between the materials. After the complete melting of ice into water, a stable S-L contact was established, and the EDL formed a stable and strong screening effect, resulting in the lowest level of charge transfer. The findings contributed to enhancing knowledge about interaction and charge transfer between different substances in dynamic phase transition scenarios. It could also provide valuable insights into the optimization and advancement of CE-based triboelectric nanogenerators for energy harvesting and self-powered sensing.

Keywords: Contact electrification; Phase transition; Electrical double layer; Triboelectric nanogenerator

Introduction

Contact electrification (CE) is a phenomenon where objects acquire an electric charge when they come into contact and then separate [1,2]. Around 600 B.C., the ancient Greeks recorded that an attractive force is created when the resin is rubbed against fur, which was the first discovered phenomenon of CE. For 2600 years, from the wool processing industry in Medieval Britain, across the textile industry during the first industrial revolution to the semiconductor foundry today, CE has had a profound impact on human life, but most of them were negative. Thus, the research on CE has predominantly focused on mitigating or reducing its negative impact. Until 2012, the triboelectric nanogenerator (TENG) based on the coupling effect of CE and electrostatic induction was first invented to exploit the positive impacts of CE for energy harvesting and self-powered sensing [3–9]. This marked a shift towards exploring the potential benefits and

* Corresponding authors.
E-mail addresses: Wang, Z.L. (zhong.wang@mse.gatech.edu), Wei, D. (weidi@binn.cas.cn).
[1] These authors contributed equally to this work.

 https://doi.org/10.1016/j.mattod.2024.03.013

applications of CE. However, the inherent mechanism of CE remains in mystery. It is commonly believed that the transfer of charges between two materials can occur through three main pathways: electron transfer [10–13], ion transfer [14–17], and material transfer [18,19]. However, the intricate details of these mechanisms are still not fully understood. Further research and exploration are needed to unravel the true nature of CE.

In the recent study of solid–solid (S-S) CE, the CE and triboelectric charging process in metal-dielectric interfaces under different thermal conditions were investigated [20–22]. It was found that the charge transfer process at the nanoscale follows a modified thermionic emission model, and an electronic cloud potential well model was proposed to explain the electron transfer phenomenon in the process of frictional charging [23–25]. The main conclusion drawn from the findings was that electron transfer is the major mechanism behind S-S interface CE. When the interatomic distance between the two materials is smaller than the normal bonding length in the repulsive region (approximately 0.2 nm), electron transfer could occur at the contact interface [26]. Furthermore, in recent studies on solid–liquid (S-L) CE, a new approach was employed by heating the substrate to dissipate electrons [27]. This approach provided the first microscopic evidence showing that both electrons and ions are crucial components of the frictional charging charge carriers at the S-L interface [28–30]. Additionally, as the ion concentration increased, ions tightly adsorbed to the solid surface would generate a screening effect, reducing the transfer of charge during the S-L CE process [31]. Based on these findings, a "two-step" model for the electrical double layer (EDL) formation was proposed [27,31,32]. This model not only explained the essence of the origin of the EDL as electron transfer at the contact interface but also resolved the controversy regarding whether electrons or ions act as the interface charge carriers. It enriched the fundamental understanding of the EDL [33]. Therefore, the charge transfer mechanism of CE has been extensively studied. However, most of these studies were based on steady-state contacts between S-S or S-L interfaces. Phase transition exists ubiquitously in nature, the changes in material structure and properties during phase transitions could have significant effects on CE. Studies have been conducted on the effects of transitioning from the glassy to the rubbery on CE [34],but this area remained largely unexplored.

In this paper, the charge transfer between typical crystal ice and the dielectric material during its melting process was studied in depth to determine the effect of phase transition on CE [35]. Ice and water provide us with a convenient platform to investigate CE at the transition interface in an ambient environment as they are of the same material. Initially, during the early stages of ice melting, S-S contact between the ice and dielectric material played a dominant role in charge transfer, with electron transfer being the primary mechanism. The formation of micro-droplets on the ice surface due to melting smoothed its surface and significantly increased the contact area between the materials. This led to a remarkable enhancement in charge transfer efficiency, approximately seven times higher than the initial contact between pure ice and the dielectric material. As the ice continued to melt, macroscopic liquid droplets condensed on the ice surface, establishing S-L contact with the dielectric material. At this stage, an EDL composed of ions and electrons was formed at the contact interface, creating a screening effect. This effectively reduced the net surface charge of the dielectric material and hindered further charge transfer, significantly decreasing the charge transfer between the materials. Therefore, investigating the precise variations in charge transfer during the process of ice-melting not only enhanced the comprehension of the influence of phase transitions on CE but also provided a deeper insight into the underlying charge transfer mechanisms involved. It could enable the development of more efficient energy harvesting approaches for S-S or S-L TENGs. Additionally, it could facilitate the creation of new types of self-powered sensors by leveraging the impact of phase transitions on CE, thereby, for example, offering accurate guidance for studying variations in ice layers during polar scientific expeditions.

Results and discussion

Electronegativity of ice and water

In this experiment, a single-electrode mode TENG with a three-layer sandwich-like structure was prepared, as shown in Fig. 1a. The TENG friction electrode consisted of three layers. The bottom contact layer was a dielectric PTFE film used for contact electrification with ice, where the ice was frozen using DI water with a conductivity of 0.055 μS/cm. The middle layer was a conductive copper layer serving as the electrode for electrostatic induction, and the top layer was a transparent thin Polymethyl methacrylate (PMMA) substrate. The hydrophobic PTFE film wrapped the copper film to prevent oxidation caused by contact with the copper film. The bottom of the TENG was composed of an ice layer and a PMMA mold. By controlling the linear motor, the contact force was maintained at 30 N, the separation gap at 8 mm, and the frequency at 2 Hz. This ensured continuous contact and separation of the friction electrode from the ice layer, resulting in the generation of triboelectric charges [36–38], as shown in Fig. S1a. Initially, there was no contact or friction between the PTFE film and the ice layer, and no triboelectric charges were generated, as shown in Fig. S1a I. When the PTFE film fully contacted the ice surface, triboelectric charges of equal and opposite polarity were generated due to the different abilities of the PTFE film and ice to gain and lose electrons, as shown in Fig. S1a II. After applying external force and separating the two friction layers, a potential difference between the PTFE film and the ice layer generated charges on the back conductive layer of the PTFE film, which were then collected by external instruments, as shown in Fig. S1a III. Triboelectric charges were continuously generated through electrostatic induction in the TENG until the potential reached equilibrium within the device, as shown in Fig. S1a IV. In the reverse scenario, when the two friction layers gradually approached each other, reverse charges were collected, as shown in Fig. S1a V. Similarly, when water did not come into contact with the PTFE film, no triboelectric charges were generated (Fig. S1b I). Applying external force brought water into contact with the PTFE film, generating triboelectric charges (Fig. S1b II). After separating the PTFE film and water, a potential difference between them generated charges on the back conductive layer of the PTFE film, which were then collected by external instruments, as illustrated in Fig. S1b III. Continuous

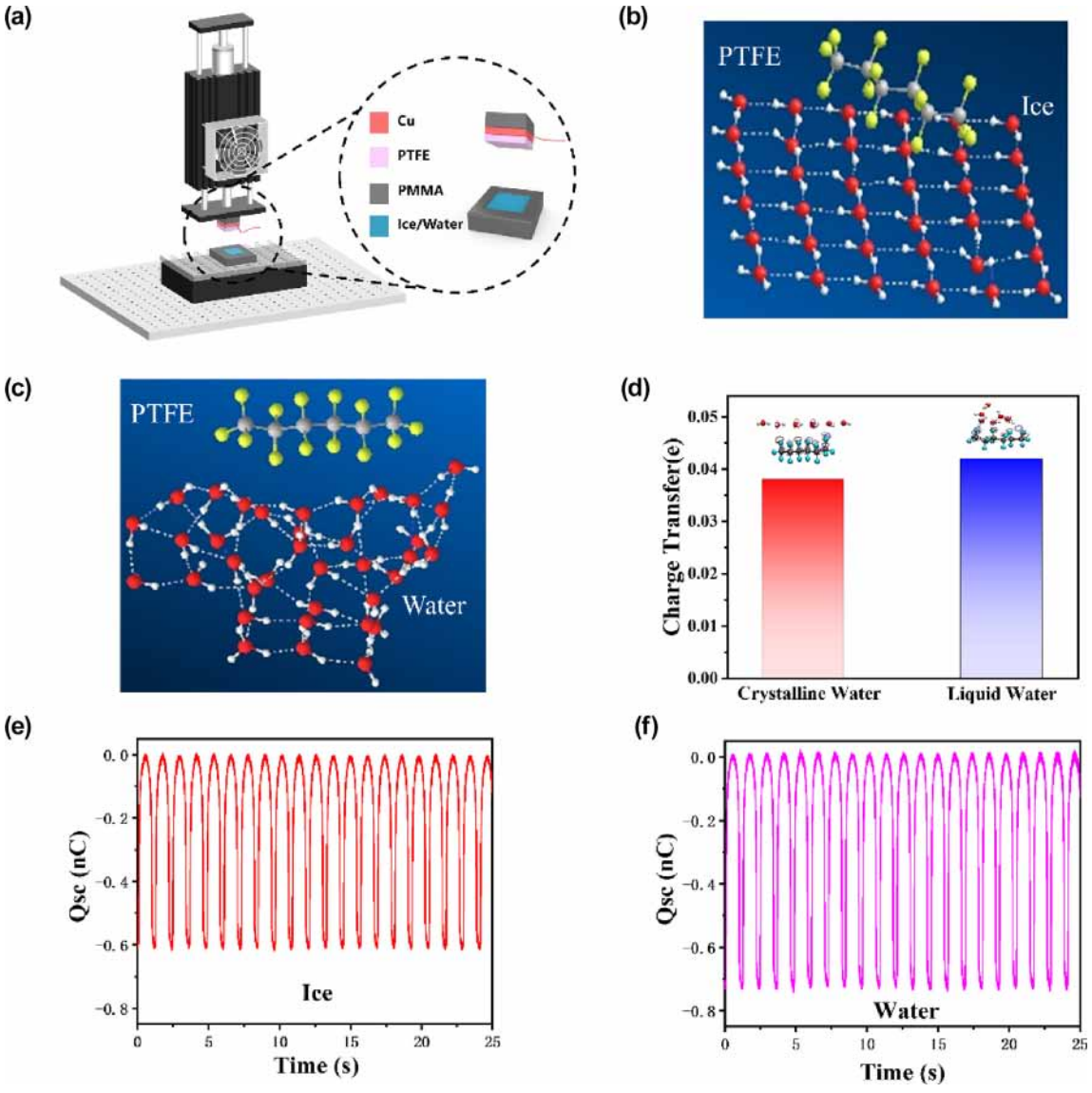

FIG. 1

The structural design of TENG and the triboelectric series for ice and water. (a) Diagram of the single-electrode mode TENG composed of a vertical linear motor.(b) Simulation diagram of PTFE contacting and separating from liquid water in contact electrification. (c) Simulation diagram of PTFE contacting and separating from ice in contact electrification. (d) Theoretical calculation of the magnitude of transfer charge during contact electrification between ice and liquid water. (e)-(f) Transfer charge magnitude with TENG in contact with water and ice under identical conditions.

generation of triboelectric charges through electrostatic induction occurred in the TENG until the potential reached equilibrium within the device, as depicted in Fig. S1b IV. In the reverse scenario, as the two friction layers gradually approached each other, reverse charges were collected, as shown in Fig. S1b V.

Previously, a significant amount of research had been conducted to explore the triboelectric properties of water, with some studies also investigating the CE of ice [24,31,39–41]. However, there were limited investigations on the triboelectric properties during their phase transition. To better understand the CE occurring during the phase transition of water and ice, it was necessary to determine their properties such as electronegativity. The magnitude of charge transfer between crystalline water (monolayer ice) and liquid water with dielectric materials during the CE process was computationally assessed using COMSOL Multiphysics. In Fig. 1b, c, to ensure a consistent PTFE chain, it is modeled as a PTFE chain with 6 carbon atoms. When working in ice form, ice formed a regular lattice structure through hydrogen bonds. On the other hand, in liquid form, water molecules were arranged irregularly, allowing for movement and collisions, constantly changing their relative positions. Water molecules in both ice and liquid water continuously came into contact and separated from PTFE. When reaching a stable state, the transferred charge quantity was recorded. As shown in Fig. 1d, the transferred charge quantity for ice was 0.38 e, and for water, it was 0.42 e. The transferred charge quantity between ice and dielectric material, as well as water and dielectric material, differed by only 10 %. To further clarify the electronegativity of ice and water, experiments were conducted. Under the same environmental

conditions, including temperature, the transferred charge quantity between ice and PTFE film, using the apparatus shown in Fig. 1a, was 0.6 nC, while the transferred charge quantity between water and PTFE film was 0.68 nC. The transferred charge quantity of water was approximately 10 % greater than that of ice, consistent with the results obtained from Multiphysics simulations, as shown in Fig. 1e, f. The electronegativity of water and ice might be comparable because of the similar quantity of triboelectric charge produced. Based on the magnitude of the transferred charge quantity, the triboelectric series for water should be between Nylon and ice (Fig. S2). Therefore, the triboelectric series from positive to negative, as shown in Fig. S3, was Nylon, water, ice, and PTFE [41].

Variations in charge transfer during the phase transition process

In Fig. 2a, when the environmental temperature was 20 °C, ice continuously absorbed heat from the environment, leading to melting. In the four stages of ice melting, "ice" referred to the state where water molecules crystallized into ice (Fig. 2a I); "initial melting" indicated the stage where liquid water began to appear at the environmental temperature (Fig. 2a II); "Partial melting" described the stage where the amount of liquid water increased but some regions still maintained ice (Fig. 2a III); "Complete melting" referred to the stage where all the ice was completely converted into liquid water(Fig. 2a IV). The transferred charge quantity of the ice-based TENG gradually increased. As the ice kept melting, the transferred charge quantity reached its peak, six times higher than the initial transferred charge quantity observed when the ice was not melted. Subsequently, as the ice continued to melt, the transferred charge quantity began to decrease. After decreasing to a certain extent, the transferred charge quantity stabilized, reaching an equilibrium state. Both short-circuit current and open-circuit voltage were tested separately (Fig. S4, S5). During the process of ice-melting into the water, as the ice changed from −20 °C to 20 °C, the transferred charge quantity of the TENG continuously changed along with the temperature variations. Therefore, TENGs were created using ice at −20 °C, −10 °C, −5 °C, 0 °C, and water at 0 °C, 5 °C, 10 °C, and 20 °C for testing their transferred charge quantity (Fig. S6). It was found that both water and ice exhibited a decrease in the transferred charge quantity as the temperature increased. When the temperature was −20 °C and 0 °C respectively, the transferred charge quantities of ice were 0.61 nC and 0.41 nC. This might be due to that the resistance value of the TENG increase with temperature elevation [41]. Additionally, it was observed

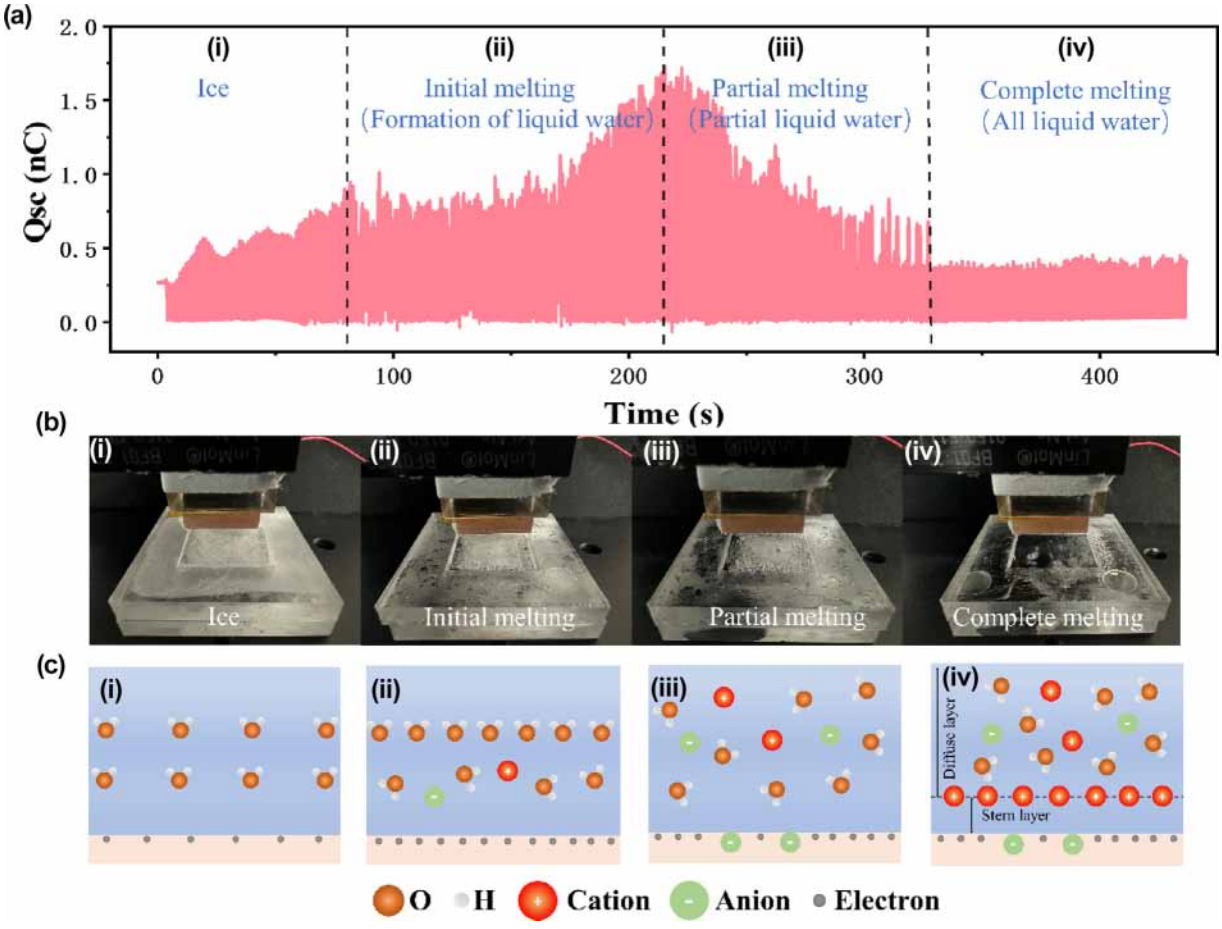

FIG. 2

The changes in the transferred charge quantity during the ice-melting process and the principles behind the formation of the EDL. (a) The variation in transfer charge magnitude during the process of ice-melting into water. (b) Phase diagram of ice-melting at different stages. (c) The formation and mechanism of the EDL in contact electrification during phase transition processes.

that when both ice and water were at 0 °C, the transferred charge quantities were 0.41 nC and 0.62 nC, respectively, with only a 33 % difference in the transferred charge quantity.

When the ice had not yet melted, PTFE film contacted the ice, as shown in Fig. 2b I. In the process of CE, only electron transfer is involved in the S-S CE as illustrated in Fig. 2c I. As the ice gradually melted, a small amount of water appeared on the ice surface (Fig. 2b II). With the melting of the ice, free water molecules and ions emerged (Fig. 2c II). In the S-L CE process, the EDL was typically formed, which influenced the behavior of S-L CE, including charge transfer and accumulation. As the ice continued to melt, a substantial amount of water was observed on the ice surface (Fig. 2b III). Owing to the contact at the S-L interface and the thermal movement of the liquid, involving molecules and ions such as H_2O, cations, and anions, numerous collisions occurred (Fig. 2c III). These collisions resulted in electron transfer between the solid atoms and water molecules due to the overlap of their electron clouds, leading to ionization reactions on the solid surface [27,42]. Both electrons and ions were generated on the surface, with electron transfer taking precedence. Due to electrostatic interactions, oppositely charged ions from the liquid were attracted to the charged surface, forming the EDL, as shown in Fig. 2c IV. Based on the research by the Wang et al., the presence of the EDL restricted the free movement of electrons and ions in the liquid near the solid surface, thereby slowing down the transfer of charges [42,43]. Simultaneously, the formation of the EDL caused an adjustment in the charge distribution on the solid surface. This adjustment could reduce or shield the free charges on the solid surface, creating a screening effect. Therefore, during the partial melting process of ice, the EDL continued to form, gradually creating a screening effect, leading to a gradual decrease in the transferred charge quantity (Fig. 2a III). In the complete melting of ice, the EDL had fully formed, resulting in the transferred charge quantity reaching an equilibrium state (Fig. 2a IV). Simultaneously, a water film could have formed on the PTFE surface, but due to the complete establishment of the EDL, the subsequent formation of the water film was considered to have negligible effect on the experimental results.

Simulation of charge transfer in PTFE with different C-chain lengths

To explore the phenomenon of increasing charge during the process of ice melting, the transferred charge quantity of PTFE with different C-chain lengths in contact with ice and water was further calculated using COMSOL Multiphysics. (Note S1 in the Supplementary Material)One uses internal coordinates (opt) to simulate liquid water molecules, and the other uses Cartesian coordinates (opt = Cartesian) to simulate crystalline water molecules. The growth of PTFE's C-chain represented the increasing contact area during the ice-melting into water process, leading to the continuous generation of TENG as liquid water came into contact, increasing the contact area during the electrification process. As shown in Fig. 3a, b, and c, with PTFE C-chains of 6, 9, and 12, respectively, in contact with ice, water molecules formed stable structures through hydrogen bonding (Fig. S7a, b). Ice continuously contacted and separated from PTFE, and the transfer charge was calculated when reaching a stable state. As the C-chain continued to grow, the effective contact area between ice and PTFE increased. This expansion in contact area enhanced CE, leading to a gradual increase in the transferred charge quantity. (Fig. 3g) When the C-chain length of PTFE was 6, the transferred charge quantity was 0.021 e. With an increase in the PTFE C-chain length to 9, the transferred charge quantity rose to 0.051 e. When the PTFE C-chain length reached 12, the transferred charge quantity increased further to 0.084 e. With the increase in the C-chain length of PTFE, the transferred charge quantity between ice and PTFE linearly increased. When the C-chain length of PTFE was 12, the transferred charge quantity was 400 % of the transferred charge quantity when the C-chain length was 6. When ice was replaced with liquid water, PTFE with C-chains of 6, 9, and 12 underwent contact and separation (Fig. 3d, e, and f). Water molecules exhibited irregular arrangements and constant motion (Fig. S7c, d). However, due to the sufficient contact during S-L CE, the transferred charge quantity between water and PTFE remained relatively stable with little variation. In Fig. 3h, when the C-chain length of PTFE was 6, the transferred charge quantity was 0.113 e. With an increase in the PTFE C-chain length to 9, the transferred charge quantity rose to 0.121 e. When the PTFE C-chain length reached 12, the transferred charge quantity increased further to 0.125 e. This indicated that in the case of water, due to a more thorough S-L CE, the transferred charge quantity remained relatively stable. In the case where the longest C-chain of PTFE was 12, the difference in transferred charge quantity between ice and PTFE and water and PTFE was 33 %, consistent with the experimental data.

Therefore, when the ice had not melted, only S-S contact occurred between the ice and the PTFE film during the contact process. As the ice gradually melted, the generation of water resulted in a transition from S-S contact to the coexistence of S-L and S-S contact, thereby increasing the effective contact area with the PTFE film. The increase in effective contact area led to a continuous increase in the transferred charge quantity. After a certain degree of ice melting, due to the limited area of the PTFE film, the rate of increase in contact area gradually decreased and reached a saturation point, resulting in a gradual reduction in the increase of the transferred charge quantity. Simultaneously, with the formation of the EDL, the shielding effect of the EDL inhibited the transfer of charge, gradually reducing the transferred charge quantity. After the complete formation of the EDL, it reached an equilibrium state.

Impact of temperature, hydrophilicity, and ion concentration on phase-transition-based TENG

To further elucidate the reasons for the variation in the transferred charge quantity during the phase transition process of ice-melting into water by manipulating the environmental temperature to accelerate the speed of the phase transition process. At the environmental temperature of 20 °C, the maximum transferred charge quantity reached 1.75 nC in 214 s (Fig. 4a). Increasing the ambient temperature to 40 °C expedited the melting of ice, reaching the maximum transferred charge quantity of 1.21 nC in 105 s (Fig. 4b). Further elevating the ambient temperature to 60 °C resulted in reaching the maximum transferred charge quantity in only 98 s, but the value decreased to 0.58 nC (Fig. 4c). The time required for the transferred charge quantity to reach its maximum value during the ice melting process was

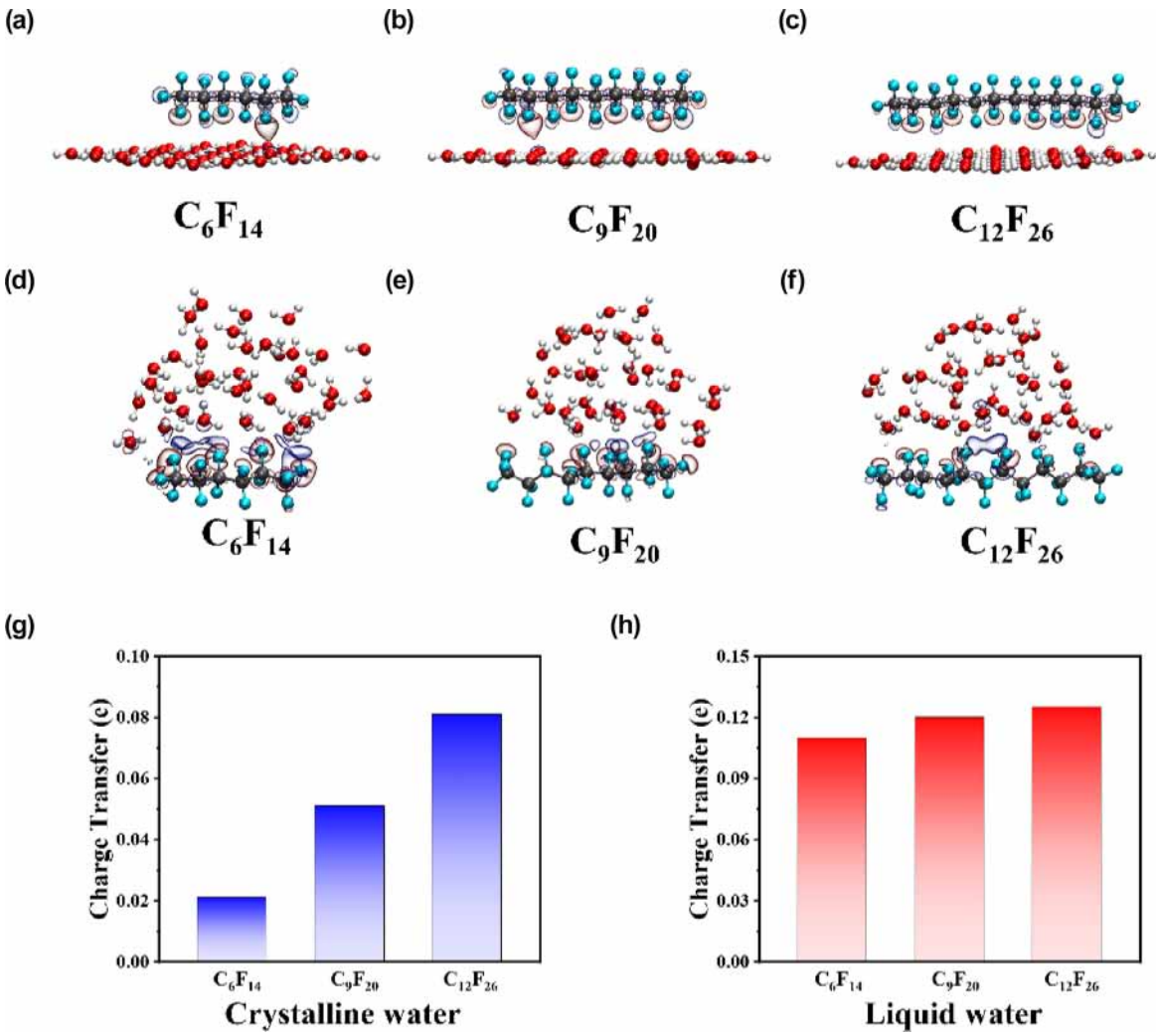

FIG. 3

The increase in the contact area between ice and water with PTFE and its impact on the change in the transferred charge quantity. (a)–(c) Contact electrification between PTFE with C-chain lengths of 6, 9, and 12 and crystalline water(monolayer of ice). (d)–(f) Contact electrification between PTFE with C-chain lengths of 6, 9, and 12 and liquid water. (g)–(h) Contact electrification transfer charge magnitude between PTFE with different carbon chain lengths and liquid water and ice.

measured. The accelerated phase transition due to the higher ambient temperature led to faster melting of ice into water, and increased contact area during triboelectrification with the presence of water, reducing the time to reach the peak transferred charge quantity. However, the elevated temperature and the appearance of liquid water also caused the rapid formation of the EDL. The shielding effect of the EDL might reduce the peak transferred charge quantity. The increase in temperature not only accelerated the melting of ice but also affected the transfer and dissipation of electrons [27]. However, in this study, the temperature did not reach the level required for the decay of surface charge. The increase in temperature affected the CE of PTFE [44], however, the EDL had already formed with stabilized transferred charge capability before reaching the glass transition temperature of PTFE. Next, the PTFE film was replaced with a more stable FEP film as shown in Fig. S8, and measured its potential during three different states: ice, ice-water mixture, and water, when in contact with the ice layer. The observed trend of potential changes aligned with the trend of the transferred charge quantity, as shown in Fig. S9. During the plasma treatment of PTFE films, excited oxygen ions and radicals generated could undergo oxidation reactions with the fluorine atoms on the surface, resulting in the formation of hydroxyl (—OH) or carboxyl (—COOH) groups, as illustrated in Fig. S10. SEM analysis in Fig. S11 demonstrated the surface changes after plasma treatment. Subsequently, the contact angle of the treated PTFE film was measured, revealing its transition to a hydrophilic surface, as depicted in Fig. S12. At a constant environmental temperature of 20 °C, friction electrodes were manufactured using Plasma-treated PTFE film, and the transferred charge quantity was tested. Compared to untreated PTFE film, the time to reach the peak charge output was shortened to only 77 s, and the peak transferred charge quantity was reduced to only 0.46 nC. The transformation of PTFE film from hydrophobic to hydrophilic increased the effective contact area between the droplet and the surface, shortening the time to reach the peak. However, the hydrophilic surface caused the droplet to adhere to the PTFE film surface, resulting in a rapid decline in the transferred charge quantity.

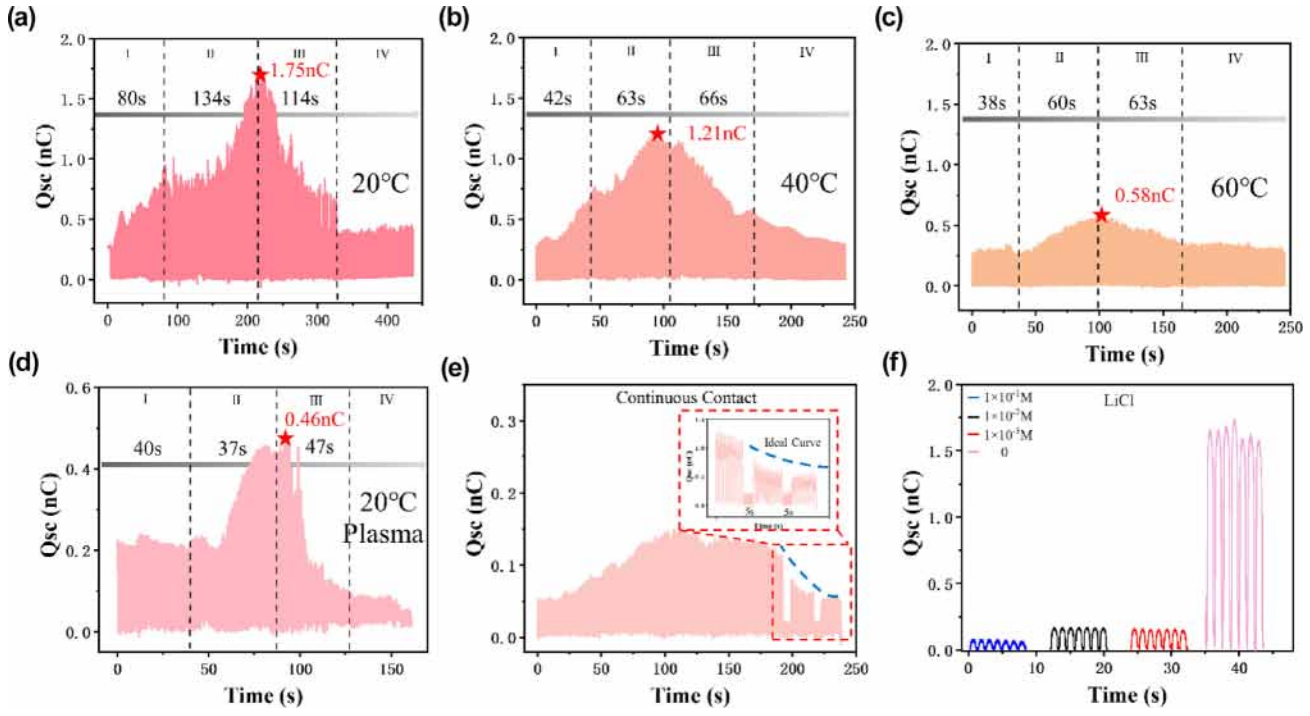

FIG. 4

The impact of temperature, hydrophilicity, and ions on the transferred charge quantity. (a)–(c) The change in transfer charge during the process of ice-melting into water at different ambient temperatures of 20 °C, 40 °C, and 60 °C.(d) The change in transfer charge of hydrophilic-treated PTFE during the process of ice-melting into water (e) The change in transfer charge of PTFE in continuous contact with ice. (f) The transfer charge during the melting process of ice made from solutions of different concentrations of LiCl.

Additionally, in Fig. 4e, continuous contact for 5 s was made with PTFE film and ice-water mixture as the transferred charge quantity approached its peak. It was observed that the actual transferred charge quantity rapidly decreased compared to the ideal transferred charge quantity, followed by a gradual stabilization. Continuous contact with water caused the rapid formation of the EDL, leading to a shielding effect and a decrease in the transferred charge quantity. As the content of water gradually increased, the contact area between the PTFE film and water saturated, and after the complete formation of the EDL, the transferred charge quantity remained stable. The variation in ion concentration could alter the transferred charge quantity of S-L contact. According to the research conducted by the Wang group, due to the shielding effect of free ions, the transfer charge during the S-L CE process decreased with the increasing ion concentration [42]. Therefore, we explored the potential influence of adding ions to ice on the amount of the transferred charge quantity. The ice layers were prepared from LiCl using the low-temperature freezing method, with each solution having concentrations of 0.1 mol/L, 0.01 mol/L, and 0.001 mol/L. They were combined with the PTFE friction layer to create TENGs, and the differences in their transferred charge quantities were observed. The TENG transferred charge quantity for different ion concentrations of LiCl was illustrated in Fig. 4f. As mentioned earlier, the introduction of ions could alter the electron transfer between surfaces. With the increase in ion concentration, there was a decrease in the amount of the transferred charge quantity, as depicted in Fig. 4f. With the increase in ion concentration, changes in the amount of the transferred charge quantity were observed. When the concentration increased from 0.001 mol/L to 0.01 mol/L, the difference in the transferred charge was not significant. However, upon further increasing the concentration to 0.1 mol/L, there was a substantial decrease in the transferred charge quantity, approaching 0. This indicated that within a lower range of ion concentrations, the change in the transferred charge quantity was relatively small. Nevertheless, once the concentration reached a certain threshold, the transferred charge quantity significantly decreased. Additionally, we noted that when the solution contained LiCl, regardless of the concentration, the transferred charge quantity was consistently less than that of DI water. This suggested that the presence of LiCl, irrespective of its concentration, led to a reduction in the transferred charge quantity compared to DI water. As the LiCl solution is introduced, more ions come into play, leading to ion transfer. However, when the ion concentration becomes too high, there is a certain competition between ions and electrons in the transfer process, which inhibits electron transfer to some extent. Additionally, the introduction of ions accelerates the formation of the EDL, and the shielding effect of the EDL also inhibits electron transfer. To further investigate the influence of the EDL on charge transfer, a model for the formation of the EDL in ice layers composed of different ions was established. As shown in Fig. S13a, H^+ and OH^- ions in the ice layer made from deionized water play a crucial role in the formation of the EDL. When the ice formed from LiCl solution continuously melts, a large amount of Li^+ and Cl^- appeared, resulting in the faster formation of the EDL, and the shielding effect was enhanced. This more effectively inhibited the transfer of

electrons, leading to a decrease in the transferred charge quantity (Fig. S13b).

Therefore, concluding that, when the friction layer contacted the ice layer, only S-S CE existed. As the ice layer melted and water droplets appeared, the contact area increased, gradually leading to the emergence of S-L CE. Additionally, due to the slow formation of the EDL at lower temperatures and when the content of liquid water was low, the EDL did not fully form. With further melting of the ice layer and an increase in the content of liquid water, the EDL gradually formed and exerted an inhibitory effect on charge transfer, resulting in a decrease in the transferred charge quantity. After melting to a certain extent, the contact area reached a saturation point. When the EDL was fully formed, the transferred charge quantity reached an equilibrium state.

Phase-Transition-based monitoring sensor

The testing setup for the contact-separation scenario was shown in Fig. 5a, illustrating a single-electrode mode TENG formed by the PTFE film friction electrode connected to a vertical linear motor. The initial temperature of the ice layer was −20 °C and triboelectric charges were continuously generated through the contact-separation between the PTFE film and ice. By adjusting factors such as temperature, hydrophobicity/hydrophilicity, and contact time, the variation in charge transfer during the ice-melting process was further enhanced (Fig. 5b). As the ice continued to melt, the transferred charge quantity initially increased to a peak, then decreased, eventually reaching a stable state. Due to the lightweight and flexibility of the manufactured TENG, it had tremendous potential in wearable applications. Additionally, it could effectively detect changes in charge transfer during the ice-melting process. Therefore, the TENG could be worn on the human body, allowing real-time monitoring of ice-melting when individuals walked or worked on ice surfaces, contributing to the safety of polar workers. Furthermore, the TENG could be utilized to accurately guide the study of ice layer changes during polar scientific expeditions. The alert system during the process of someone walking on the ice as it melts was illustrated in Fig. 5c. These signals were received and analyzed in real time through terminal devices. As the ice melted, the TENG's output performance showed fluctuations in both increase and decrease. Threshold sensors were utilized, and during the ice melting process, signal fluctuations reaching the threshold were detected. When these signals changed, wireless alert devices could utilize this information to detect real-time hazards, issuing alerts to prompt polar scientists to avoid dangerous areas and ensure their safety. To make the experiment more realistic, the TENG was attached to the soles of a person's shoes, continuously coming into contact and separating with ice in different states as the person walked, generating triboelectric charges (Fig. 5d). This was used to identify the real-time condition of the ice surface when the wearer walked on it. When a person walked on the non-melting ice surface, the transferred charge quantity was 0.6 nC. However, under the same conditions, when walking on the melting ice surface, the transferred charge increased to 2.5 nC. In the area where the ice melted extensively into the water, the transferred charge quantity decreased to 0.4 nC (Fig. 5e). Based on the varying transferred

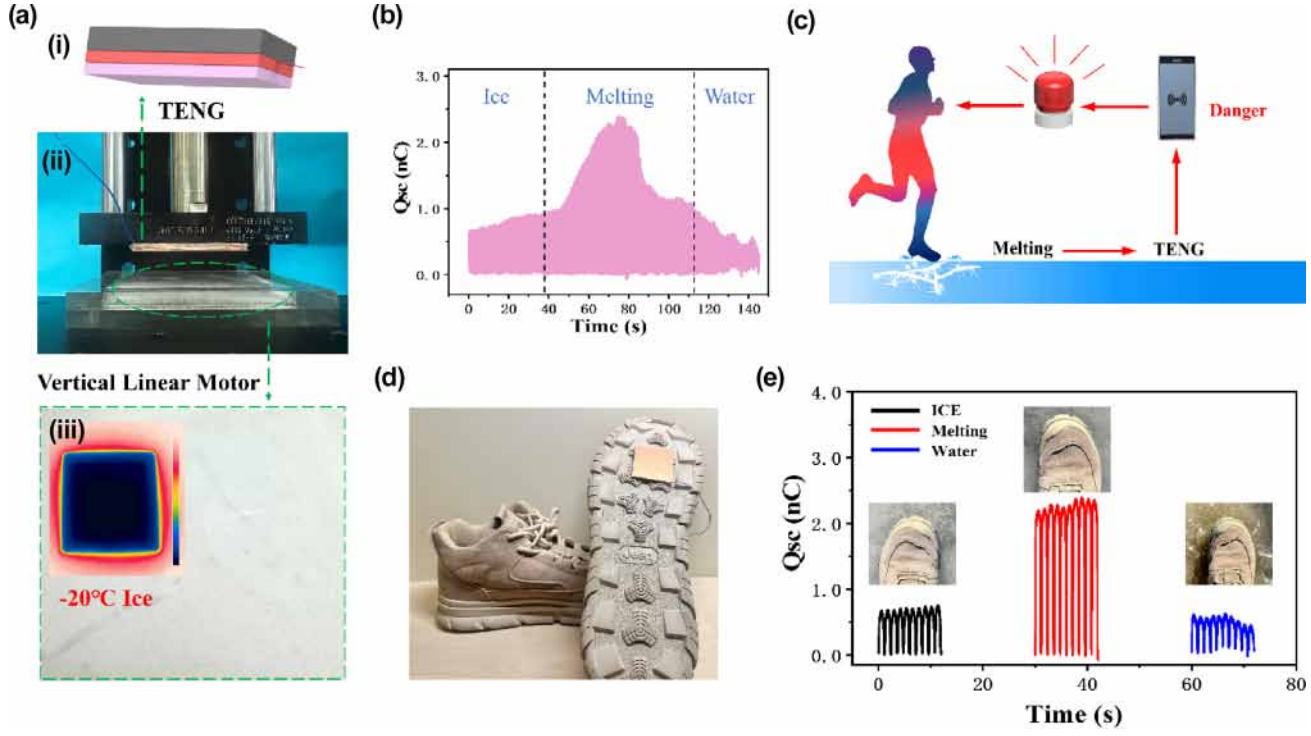

FIG. 5

Phase-transition-based monitoring sensor. (a) The experimental setup depicts the vertical linear motor, ice layer, and the manufactured TENG. (b) The variation in output charge during the ice-melting process. (c) Schematic diagram of real-time monitoring and alert sensor for ice melting. (d) Photo of the assembly and connection of the TENG device at the bottom of snow boots. (e) The transfer charge of the ice as the wearer walks in different conditions.

charge quantity, the state of the ice underfoot during walking could be determined. Therefore, by adjusting the sensing range of the receiving module, real-time monitoring of the ice surface could be achieved using the differences in electrical output, thereby ensuring the personal safety of polar workers.

Conclusion

In conclusion, this experiment investigated changes in CE and charge transfer during the ice-melting process, exploring variations in CE when a substance undergoes phase transition. Through experimental measurements and theoretical calculations, it was observed that during the ice-melting process, there was a gradual increase in the transferred charge quantity reaching a peak, followed by a decrease towards equilibrium. The results indicated that as the ice melts, there was a gradual transition from S-S contact to S-L contact, leading to an increase in contact area and a subsequent rise in the transferred charge quantity. With the gradual increase of liquid water and the continuous occurrence of CE, the contact area reached saturation, and ions, electrons, and water molecules were introduced. These ions, electrons, and water molecules contributed to the continuous formation of the EDL. The shielding effect of the EDL resulted in a reduction of the transferred charge quantity, and after the complete formation of the EDL, the transferred charge quantity reached a stable state, maintaining equilibrium. This study represented the first experimental investigation into the changes in CE during the phase transition of the same substance. It explored the formation mechanism of the EDL and the differences between S-S CE and S-L CE. Additionally, leveraging the impact of phase transition on CE could facilitate the development of precise self-powered sensors, thereby providing accurate guidance for studying variations in ice layers during polar scientific expeditions.

Experimental section

Materials

The 50 μm-thick Polytetrafluoroethylene (PTFE) film (industrial grade) was purchased from Aladdin, while the 5 mm-thick Polymethyl methacrylate (PMMA) film (industrial grade) was acquired from Alibaba. The 50 μm-thick industrial-grade fluorinated ethylene propylene (FEP) film was purchased from Aladdin. Furthermore, all the chemical reagents used in this experiment are of analytical grade and require no further treatment.

Fabrication of the triboelectric nanogenerators

Attach a copper foil strip (1.5 cm × 1.5 cm) to one side of the PTFE film, and affix copper wires to the other side to create the PTFE friction electrode. Cut an inner groove (2 cm × 2 cm × 0.5 cm) into a PMMA mold (4 cm × 4 cm × 1 cm) and fill it with deionized water (DI water) with a conductivity of 0.055 μS/cm. Place it on refrigerator to create an ice layer. To ensure consistent surface roughness during the freezing process, a PMMA cover was added above the mold. Gradually freeze the water layer into ice by maintaining the temperature below −20 °C. Assemble the two devices to form a single-electrode TENG.

Characterization and measurement

The electrical output performance of the TENG, including Voc, Isc, and Qsc, was tested using a programmable electrometer (Keithley 6514). Real-time data collection was achieved through a software platform built based on LabView. The vertical uniaxial motor (Linmot HC14-10) was used to apply variable vertical force. Surface potential was measured using Kelvin probe force microscopy (KPFM 347). The surface morphology of PTFE was characterized using a scanning electron microscope (FESEM) and a contact angle meter.

CRediT authorship contribution statement

Yu Wei: Writing – review & editing, Writing – original draft, Project administration, Methodology, Investigation, Formal analysis, Data curation. **Xiang Li:** Writing – review & editing, Writing – original draft, Validation, Supervision, Data curation, Conceptualization. **Zhe Yang:** Validation, Software, Formal analysis, Data curation. **Jiajia Shao:** Validation, Software, Data curation. **Zhong Lin Wang:** Writing – review & editing, Project administration, Funding acquisition. **Di Wei:** Writing – review & editing, Writing – original draft, Supervision, Resources, Funding acquisition, Conceptualization.

Data availability

Data will be made available on request.

Declaration of competing interest

The authors declare that they have no known competing financial interests or personal relationships that could have appeared to influence the work reported in this paper.

Acknowledgement

This work was supported by the Beijing Natural Science Foundation (Grant No. IS23040).

Appendix A. Supplementary material

Supplementary data to this article can be found online at https://doi.org/10.1016/j.mattod.2024.03.013.

References

[1] J. Lowell et al., Adv. Phys. 29 (6) (2006) 947.
[2] B.D. Terris et al., Phys. Rev. Lett. 63 (24) (1989) 2669.
[3] F.-R. Fan et al., Nano Energy 1 (2) (2012) 328.
[4] Z.-H. Lin et al., Angew. Chem. Int. Ed. Engl. 52 (48) (2013) 12545.
[5] H. Yang et al., Nat. Commun. 10 (1) (2019) 2309.
[6] J. Nie et al., Nat. Commun. 10 (1) (2019) 2264.
[7] Y. Zou et al., Nat. Commun. 10 (1) (2019) 2695.
[8] Z.L. Wang, Nature 542 (7640) (2017) 159.
[9] Y. Liu et al., Nat. Commun. 11 (1) (2020) 1599.
[10] D.K. Donald, J. Electrochem. Soc. 115 (3) (1968) 270.
[11] H.W. Gibson, J. Am. Chem. Soc. 97 (13) (1975) 3832.
[12] M. Sakaguchi et al., J. Electrost. 72 (5) (2014) 412.
[13] C. Liu et al., Nat. Mater. 7 (6) (2008) 505.
[14] A.F. Diaz et al., Chem. Mater. 3 (6) (1991) 997.
[15] L.S. McCarty et al., Angew. Chem. Int. Ed. 47 (12) (2008) 2188.
[16] D.K. Davies, J. Phys. D: Appl. Phys. 2 (11) (1969) 1533.
[17] C.B. Duke et al., J. Appl. Phys. 49 (1) (2008) 315.
[18] R.K. Pandey et al., J. Phys. Chem. C 122 (28) (2018) 16154.
[19] H.T. Baytekin et al., Science 333 (6040) (2011) 308.
[20] J. Lowell, J. Phys. D: Appl. Phys. 8 (1) (1975) 53.
[21] W.R. Harper, Br. J. Appl. Phys. 11 (8) (1960) 324.

[22] H. Wang et al., Nat. Commun. 11 (1) (2020) 4203.
[23] S. Lin et al., Adv. Mater. 31 (17) (2019) 1808197.
[24] C. Xu et al., Adv. Mater. 30 (15) (2018) 1706790.
[25] O. Verners et al., Adv. Mater. Interfaces 10 (36) (2023) 2300562.
[26] S. Lin et al., Adv. Mater. 31 (27) (2019) 1901418.
[27] S. Lin et al., Nat. Commun. 11 (1) (2020) 399.
[28] H. Zhang et al., Matter 5 (5) (2022) 1466.
[29] W. He et al., Adv. Mater. 35 (7) (2023) 2209657.
[30] S. Lin et al., Nano Energy 76 (2020) 105070.
[31] J. Nie et al., Adv. Mater. 32 (2) (2020) e1905696.
[32] Z.L. Wang et al., Mater. Today 30 (2019) 34.
[33] X. Li et al., Matter 6 (11) (2023) 3912.
[34] A. Šutka et al., Materials Horizons 7 (2) (2020) 520.
[35] V.F. Petrenko et al., Physics of Ice, Oxford University Press, 2002.
[36] Z.L. Wang, Adv. Energy Mater. 10 (17) (2020) 2000137.
[37] H. Zou et al., Nat. Commun. 10 (1) (2019) 1427.
[38] Z.L. Wang, ACS Nano 7 (11) (2013) 9533.
[39] X. Li et al., Adv. Funct. Mater. 29 (2019) 35.
[40] C.R.S. Rodrigues et al., Nano Energy 30 (2016) 379.
[41] N. Luo et al., Nano Energy (2022) 97.
[42] S. Lin et al., Chem. Rev. 122 (5) (2022) 5209.
[43] F. Zhan et al., ACS Nano 14 (12) (2020) 17565.
[44] L. Zhang et al., Nano Energy 78 (2020) 105370.